This is a preprint, the final version is subject to change, of the American Mineralogist (MSA)
Cite as Authors (Year) Title. American Mineralogist, in press.
DOI: https://doi.org/10.2138/am-2019-6829

REVISION 1

The Effect of Oxidation on the Mineralogy and Magnetic Properties of Olivine

Joseph Knafelc[1], Justin Filiberto[1,2*], Eric C. Ferré[1,3], James A. Conder[1], Lacey Costello[1], Jake R. Crandall[1,4], M. Darby Dyar[5], Sarah A. Friedman[1,6], Daniel R. Hummer[1], and Susanne P. Schwenzer[7]

[1]Department of Geology, Southern Illinois University, 1259 Lincoln Dr, Carbondale, IL 62901, USA

[2]Lunar and Planetary Institute, USRA, 3600 Bay Area Blvd, Houston, TX 77058, USA
*JFiliberto@lpi.usra.edu

[3]School of Geosciences, University of Louisiana at Lafayette, Hamilton Hall, Room 323, 611 McKinley St.Lafayette, LA 70501, USA.

[4]Eastern Illinois University, Department of Geology and Geography, Physical Science Building, 600 Lincoln Ave., Charleston, IL 61920

[5]Department of Astronomy, Mount Holyoke College, 50 College St., South Hadley, MA 01075

[6]Department of Biological & Physical Sciences, Montana State University Billings, 1500 University Drive, Billings, MT 59101, USA

[7]School of Environment, Earth, and Ecosystem Sciences, The Open University, Walton Hall, Milton Keynes MK7 6AA, UK

Abstract: Although nucleation of magnetite and/or hematite along dislocations upon oxidation of olivine has been observed by many workers, the effect of oxidation on the magnetic properties of the sample with specific mineralogical alterations has not been studied. Therefore, we investigate this problem using a set of time series 1 bar oxidation experiments at 600 °C and 900 °C. Results show rapid olivine oxidation and alteration at both 600 and 900 °C, forming magnetite and hematite associated with a change from paramagnetic to ferromagnetic behavior after oxidation. Magnetite and hematite nucleate along dislocations and impurities in the crystal structure, along with surface coatings and within cracks in the crystals.

Fresh, unaltered mantle xenoliths containing magnetite have been interpreted as having formed in cold tectonic regimes in the mantle, rather than through oxidation during or after ascent. Mantle xenoliths rapidly ascend through the mantle with estimates of ascent of up to 90 km/hour (3 GPa/hour) based on the diffusion profile of water in mantle olivine. The rates correspond to xenoliths ascending through the mantle over hours and not days or weeks. Our results show that olivine oxidation and alteration can occur in days to weeks at 600 °C and within minutes at 900 °C. Therefore, if the xenolithic material is transported to the surface in a cold magma (at temperatures ≤600 °C), then the time scale of ascent is likely not long enough for oxidation to cause magnetite formation or a ferromagnetic signature to occur. However, if the material is transported in a hot oxidized basaltic magma (with temperatures ≥900 °C), then oxidation can cause magnetite formation and a ferromagnetic signature.

Keywords: olivine, oxidation, hematite, magnetite, magnetic properties, xenoliths

Introduction

Olivine is typically the first mineral to crystallize from mafic and ultramafic magmas and is also the first mineral to be modified in a typical alteration and oxidation sequence (e.g., Bowen 1928; Goldich 1938; Hausrath et al. 2008). Consequently, its degradation state in a rock can be used as proxy for the length of time of alteration and oxidation (Hausrath et al. 2008). Olivine typically alters to magnetite or hematite under oxidizing conditions (though laihunite may also form), and iron oxyhydroxides, such as goethite, under hydrous conditions (e.g., Goode 1974; Eggleton et al. 1987; Khisina et al. 1998; Oze and Sharma 2005; Syverson et al. 2017). In a seminal paper, Kohlstedt et al. (1976) showed that magnetite and/or hematite can nucleate along dislocations upon oxidation of olivine (so called 'olivine decoration' experiments). However, this work did not investigate how oxidation affects changes in magnetic properties of the sample with specific mineralogical alterations. Therefore, we here investigate the effect of oxidation on the magnetic properties of olivine. The main motivation for combining oxidation experiments with magnetic measurements arises from the recent work by Ferré et al. (2013); (2014) and Friedman et al. (2014), which showed that fresh, unaltered mantle xenoliths contain magnetite that is interpreted as having formed in cold tectonic regimes in the mantle, as opposed to having formed through oxidation during or after ascent. Therefore, this work seeks to constrain both the rates of magnetite formation during oxidation, and how this oxidation affects magnetic properties, in order to assess if oxidation during or after ascent can account for the magnetic properties of mantle xenoliths.

Olivine dislocation decoration experiments, originally used to investigate rates of creep along dislocation as a mechanism for modeling mantle flow patterns, have also led to important insights in magnetite formation from olivine oxidation (Kohlstedt et al. 1976). These

experiments were performed at atmospheric conditions (pressure and oxygen fugacity) and a mantle-like temperature of 900 ºC for one hour. The results showed that oxidized phases formed along lattice dislocations and produced reddish-colored olivine caused by the formation of either magnetite or hematite (Kohlstedt et al. 1976). Subsequent experimental results on iron-rich olivine (Fo_{50}) showed that oxidation followed a two-step process where the fayalitic component first reacts to form magnetite, after which forsterite breaks down to form enstatite (Goode 1974). For typical terrestrial mantle olivine (~Fo_{90}), this process may either be a partial or complete reaction, replacing olivine with some combination of magnetite, pyroxene, and/or quartz (e.g., Goode 1974; Nitsan 1974).

In the presence of water, olivine oxidizes and alters to serpentine along with magnetite potentially releasing H_2 gas (e.g., Oze and Sharma 2005; Syverson et al. 2017). If magnesium is not lost, olivine may alter to saponite or nontronite (Eggleton et al. 1987). However, depending on the environment, olivine may also oxidize to hematite or goethite (Goode 1974). Alternatively, oxidation and alteration may produce both hematite and ferric iron in pyroxene in the presence of a carbon dioxide rich atmosphere, as has been suggested for Venus (Fegley et al. 1995).

Magnetite has been reported in mantle xenoliths in several studies (e.g., Wasilewski et al. 1979; Wasilewski and Mayhew 1992; Warner and Wasilewski 1995; Callahan 2009; Ferré et al. 2013; Ferré et al. 2014; Friedman et al. 2014). In some cases, magnetite occurs in thin impregnating veins due to basalt contamination. In other cases, magnetite occurs mainly along the xenolith rim and probably results from supergene serpentinization. The origin of this magnetite in mantle xenoliths is crucial to the in situ evaluation of the magnetic properties of the upper mantle.

Olivine oxidation and magnetite formation can occur via several different processes including (1) alteration and reaction with fluids after eruption of the host magma, (2) reaction with the host magma upon ascent, or (3) metasomatism at depth (e.g., Banfield et al. 1990; McGuire et al. 1991; Dyar et al. 1992; Canil et al. 1994; Luguet and Lorand 1998; Hausrath et al. 2008; Creighton et al. 2009).

(1) Alteration from reaction with a low temperature fluid specifically causes the formation of Ti-poor magnetite with maghemite, hematite, laihunite, and/or goethite (e.g., Banfield et al. 1990; Luguet and Lorand 1998).

(2) Metasomatic reactions in mantle xenoliths formed by interaction with a magmatic dike occur when the magma is significantly more oxidized than the mantle xenolith (e.g. McGuire et al. (1991)]. The Fe^{3+}/Fe^{T} ratios increased in olivine, pyroxene, amphibole, and spinel near the magmatic dike, with this change being controlled by the oxygen fugacity of the system; however in this case magnetite did not form but instead metasomatic oxidized amphibole formed (McGuire et al. 1991).

(3) Finally, oxidation may occur at depth from mantle metasomatism where water and CO_2-rich fluids in the mantle cause oxidation via a dehydrogenation reaction that transfers the charge from H and changes Fe^{2+} to Fe^{3+} (e.g., Dyar et al. 1992; Canil et al. 1994; Creighton et al. 2009; Dasgupta and Hirschmann 2010; Dasgupta et al. 2013). Such metasomatic olivine oxidation has been described in mantle xenoliths from the Kamchatka island arc where subducted slab-derived fluids oxidized the overriding mantle wedge (Ishimaru et al. 2009; Ferré et al. 2014). A recent study of the oxidation state of Fe in inclusions of ultra-high pressure majoritic garnet in diamond showed that Fe^{3+} actually increased with depth of garnet formation,

consistent with the presence of carbonated fluids oxidizing the deepest portion of the upper mantle and transition zone, and not just the shallow mantle (Kiseeva et al. 2018).

Recent studies have shown that magnetite can also be found in unaltered, unmetasomatised, and unoxidized mantle xenoliths (Ferré et al. 2013; Ferré et al. 2014). These 'fresh' mantle xenoliths show no evidence for external oxidation along high energy grain boundaries, making secondary oxidation and alteration during ascent and emplacement an unlikely process for magnetite formation (Ferré et al. 2013; Ferré et al. 2014). Further, mantle xenoliths tend to rapidly ascend from their mantle sources and likely would not have sufficient time to oxidize during or after ascent (Nixon 1987; Haggerty and Sautter 1990; Demouchy et al. 2006; Peslier et al. 2015). The rapid ascent rates of mantle xenoliths, as recorded by water diffusion signatures in the rims of mantle olivine, are on the order of up to 90 km/hr (Demouchy et al. 2006; Peslier et al. 2015). Therefore, the magnetite found in these fresh xenoliths is interpreted as having formed at upper mantle depths, particularly in cold geotherm settings such as cratons regions (Ferré et al. 2013; Ferré et al. 2014; Friedman et al. 2014). This has led to the hypothesis that the observed long wave-length magnetic anomalies (LWMA) in some craton regions may partially originate from magnetite in the uppermost mantle (Ferré et al. 2013; Ferré et al. 2014; Friedman et al. 2014). Long-wavelength magnetic anomalies (LWMA) are broad scale features of the lithospheric magnetic field with half-wavelengths that are often greater than 250 km (Thébault et al. 2010). Previous work typically assumed that the magnetic anomalies were solely derived from crustal sources in both forward and inversion models (e.g., Hemant and Maus 2005; Masterton et al. 2013) based on studies of xenoliths (Wasilewski and Mayhew

1992). However, our recent work has shown that contributions from the mantle may be up to 30 % of the LWMA signature in some cratons (Idoko, 2017, MS Thesis; Idoko et al., in review).

We therefore investigate the rate of magnetite formation from olivine at mantle temperatures to help constrain where oxidation in the xenoliths occurs, how quickly oxidation will affect not only mineralogy but also the magnetic properties, and ultimately if the uppermost mantle could contribute to LWMA. These experiments reveal whether diffusion rates of Fe in olivine limit the growth of magnetite upon ascent. We report here on a set of time series heating experiments on single grain gem quality olivine at 600 °C and 900 °C following the seminal work of Kohlstedt et al. (1976). Our experiments were done in air (see methods below), which imposes an fO_2 significantly higher than typical mantle conditions, but the results represent an upper limit in terms of formation rates.

Methods

Olivine High Temperature Oxidation Experiments:

Single gem quality olivine crystals from San Carlos, Arizona and China were purchased from mineral suppliers. Olivine crystals were investigated by optical microscopy and only those olivine that did not display any evidence for alteration (brown colorations, cloudiness, etc) were chosen for study. Olivine crystals were measured and photographed before experimentation for comparison with post experimentation (**Supplemental Figure 1**). Further, all olivine samples were measured by Vibrating Sample Magnetometer (VSM) for their magnetic properties and any sample with a ferromagnetic signature was discarded (see below for more information).

All olivine samples were placed in a box furnace at atmospheric oxygen conditions at 600 °C and 900 °C. Samples at 900 °C were placed directly on the plate in the furnace; while the

600 °C were placed in open-ended Al-crucibles to keep sample pieces together after breaking. Olivine in the 900 °C experiments broke apart during oxidation and therefore a change was made to the protocol for the 600 °C experiments in order to keep the furnace clean. The upper temperature was specifically chosen to parallel the seminal work of Kohlstedt et al. (1976), where oxidized phases grew in only one hour.

The oxygen fugacity of our experiments was indirectly controlled by atmospheric conditions. The oxygen fugacity of the atmosphere is ~ QFM + 10 (e.g., McCammon 2005), which is 10 orders of magnitude higher than mantle conditions. This was chosen on purpose as an extreme end member of how oxidizing olivine by contamination with a magma (~QFM +3 for subduction zone magmas), the crust (QFM +2-3), or the atmosphere (QFM +10) (Parkinson and Arculus 1999; McCammon 2005; Kelley and Cottrell 2009; Mullen and McCallum 2013) would affect the mineralogy and magnetic signature.

For each temperature, twelve olivine crystals were placed in the furnace and two single olivine grains were incrementally removed after 0.2, 1, 5, 25, 125, and 625 hours. Two grains were removed quickly (typically in a few seconds) at each time interval to produce repeatable results. The temperature of the furnace did not fluctuate significantly (< 20 °C) during sample removal. Fragments of fractured samples from the 900 °C experiment after 625 hours were used to make a thick section for textural analyses.

Electron Microprobe Imaging:

Backscattered electron (BSE) images and X-ray intensity maps of a thick section of fragments from the 900 °C experiment after 625 hours were taken with the Cameca SX100 electron microprobe (EMP) at the Open University (OU) for textural analyses of the sample as a representative. This sample was chosen because it contains the highest portion of oxidation. The

instrument is equipped with a Bruker EDX detector and five WDS spectrometers. Operating conditions were 20 kV accelerating voltage, 20 nA current applying the smallest possible spot size (~1 μm) for the mapping.

Raman Spectroscopy:

All oxidized samples were analyzed using a Bruker Optics, Inc. Bravo Raman spectrometer at Mount Holyoke College. Samples were run as bulk and not crushed or powdered before analyses. Samples China 21, China 12, Sc-23, and Sc-8 were not analyzed by Raman as the samples were too small to measure. The Raman spectrometer was used for acquiring mineralogical data through a dual laser (758 and 852 nm) excitation and fluorescence mitigation strategy involving successive heating of the laser. With a scan time of 10s and wavenumber range of 300-3350 cm^{-1}, each sample was run five times and the spectra were averaged. The BRAVO spectrometer software produces baseline-subtracted data.

The spectrum for each sample was analyzed by matching peaks of mineral standards from the RRUFF data base with the program Crystal Sleuth (Lafuente et al. 2016). Maghemite does not have a catalogued standard; therefore, to determine if maghemite was present in the samples, the results were compared with results with known maghemite detections (Hanesch 2009). Raman spectra from the previous experimental work show that maghemite produces peaks at 350, 500, and 700 cm^{-1}, which do not correlate to any other Fe-oxide Raman peak (De Faria et al. 1997; Hanesch 2009).

Crystal Sleuth gives a percentage for how well a spectrum matches different mineral standards. The closer the percentage is to 100, the more confidence there is that the mineral is present. Peaks matching with a confidence level of 90% are considered to be a major mineral phase in a sample. Peaks that matched between 70 and 90% to a mineral standard are considered

to be a minor mineral phase. Peaks that are matched below 70% and above 50% are considered trace (and may be at or near the detection limit depending on the Raman cross section of the mineral).

Vibrating Sample Magnetometer (VSM):

The magnetic hysteresis properties of each sample were analyzed using the Princeton Measurements Corporation Vibrating Sample Magnetometer 3900-04 (VSM) at SIU. The measurement of magnetic hysteresis, the magnetic behavior of a material in and out of an applied field, is useful in characterizing the remanence carriers of rocks. In addition, the analysis of remanence, or residual magnetism, can determine the magnetic contribution of mineral grains in a sample. Ferromagnets, sensu lato, will exhibit a strong response to a magnetic field, while parmagnetic grains will display a weak response. For the purpose of this experiment, the paramagnetic (i.e., olivine) and ferromagnetic (i.e., magnetite and hematite) contributions are of principal concern, as these are the temperature-dependent reflections of magnetic order.

1. Magnetic Hysteresis – We applied DC fields up to 1 Tesla, at room temperature. The variation of magnetization with applied ascending and descending fields follows a magnetic hysteresis loop, or plot of the variation of magnetization within a magnetic field. These experiments allow the quantification of the paramagnetic and ferromagnetic contributions. The maximum induced magnetic moment, the magnetic field of saturation (H_s) was calculated after a slope adjustment of 70 percent of the applied field. The high field data was linear in all samples studied and corresponds to the paramagnetic contribution from olivine in the samples. This paramagnetic contribution is corrected using the linear equations resulting from the 4 high field slope curves generated during ascending and descending applied fields. The average slope from each high field linear equation results in a high field slope correction. The magnetic hysteresis

parameters, magnetic saturation (M_s) which is measured after saturating a mineral in an applied field of 1-2 Tesla (T), magnetic remanence at saturation (M_r) the magnetism persisting after an applied field is reduced to zero, magnetic coercivity (H_c) the point at which magnetization is returned to zero by applying a field in a negative direction, and coercivity of remanence (H_{cr}), the reverse field that reduces M_r to zero after it is applied and removed, are plotted as ratios in Dunlop (2002) plots. These plots illustrate the nature of the magnetic domain in the system. Samples with larger M_r/M_s ratios have smaller grain sizes while samples with larger H_{cr}/H_c have larger grain sizes.

2. Isothermal Remanent Magnetization (IRM) – IRM is the remanence left in a material after a steady field (1-1000 mT) has been applied for a short time (~100 seconds) then removed. These experiments allow the distinction of mineral phases of different magnetic coercivity. In general minerals with larger coercivity (e.g., hematite) will require a larger applied magnetic field (up to 2 T and higher) to reach magnetic saturation; while minerals with a smaller coercivity (e.g., magnetite) saturate under lower field (<0.2 T). The IRM is normalized to the highest magnetic saturation for each sample in order to investigate the approach to saturation (e.g., Tauxe et al., 2015). The IRM data was used to also determine the relative proportions of each magnetic phase which contributes to the total magnetization. This was done using MAX UnMix, a program designed to separate coercivity spectra of different magnetic phases (Maxbauer et al. 2016). The derivative of the IRM normalized curves shows peaks of different coercivities corresponding to different Fe-oxide phases.

Results

For each time increment, two samples were simultaneously removed to ensure that the results would be reproducible. As described below, samples that have spent an equal amount of time in the furnace have virtually the same amount of alteration.

Textural analyses:

Before and after oxidation, samples from each time interval were photographed to show how oxidation progressed with time at a constant temperature (**Figure 1; supplemental Figure 1**). After only 12 minutes (0.2 hours) at 900 °C, the olivine samples began to shows signs of oxidation, forming red to brown coloration; however, the samples were still mostly unaltered. Samples that spent 1 hour in the furnace began to show a metallic iridescent reddish-brown coating. After 5 hours, the samples were completely altered, showed a complete metallic iridescent reddish-brown coating, and no sign of the original olivine green coloring. All samples oxidized longer than 5 hours were predominantly reddish-brown with the coloring becoming darker with time. For experiments at 600 °C, the red/brown of the olivine and production of a metallic iridescent coating followed the same pattern as the higher temperature experiments, but the alteration effects took longer time to develop (**Figure 1**).

Figure 2 displays the BSE image and X-ray element concentrations of a thick section of a sample oxidized for 625 hours at 900°C. The sample shows three distinct morphologies of oxidative alteration: 1) surface coating, 2) crack filling, and 3) within crystal lattice. The entire crystal is coated with a surface coating visible as a bright phase in the BSE image and higher iron concentration than the original olivine. Some of this surface coating has been broken away during making of the thick section. The bright/high iron phase also is evident within irregular cracks throughout the olivine grain. Finally, the bright/high iron phase also appears within the

crystal structure where it occurs as inclusions with perpendicular orientations suggesting it formed along preferred crystallographic directions within the orthorhombic olivine structure.

Mineralogy:

Mineralogy for all samples was derived from Raman spectroscopy and was dominated by olivine for all samples – including the most oxidized (**Figure 3; Table 1**). Importantly, there is no detectable alteration in the unaltered crystals. However, with increasing duration of the experiment, the Raman spectroscopy, and therefore mineralogy, showed significant changes. The Raman spectrum for the 900 °C experiments shows evidence for hematite formation after only 12 minutes and hematite appears in all experiments (**Figure 3**). Interestingly, for some of the long duration runs (>25 hours), there is also a trace amount of enstatite and quartz (**Figure 3**). This mineralogy is consistent with the reactions reported by Goode (1974), which found forsterite breaking down to iron-oxide plus enstatite and quartz. However, the Raman results contain mainly hematite with limited evidence for magnetite (**Figure 3**). This is a consequence of the temperatures of our experiments. With increasing temperatures, magnetite undergoes first a phase transition to maghemite and then a transition from maghemite to hematite (e.g., Swaddle and Oltmann 1980; De Boer 1999). Further, there is the possible presence of clinohumite ($(Mg, Fe)_9(SiO_4)_4(OH)_2$) in some samples, which is most likely a product of humidity in the room that provided water (as OH^-) to the experimental products while either conducting the experiment or upon removal from the oven.

Experimental results at 600 °C show a similar mineralogy but the alteration takes longer to occur. In the first five hours, all samples remain spectroscopically unaltered (olivine only in the Raman spectra), even though visually small brown/red patches appear (**Figure 3**). After 5 hours of oxidation, hematite is the first alteration phase to form. No other alteration phase is

found in the Raman spectra of the lower temperature experiments over the course of our experiments. This is consistent with kinetics, where higher temperatures facilitate diffusion in a solid phase and thus increase reaction progress.

Magnetic Data:

900 °C Experimental Results. Before and after oxidation, samples were analyzed using a magnetic hysteresis loop (**Figure 4**). Each sample showed paramagnetic behavior before oxidation and ferromagnetic behavior after oxidation. This change in magnetic behavior occurs after 12 minutes (0.2 hours) of oxidation and is persistent in all samples from the 900 °C experiments. Normalized IRM curves for each sample (**Figure 5**), are similar because the same ferromagnetic phase is producing the magnetic signature in each sample. The first derivative of the IRM curves shows where the change in slope occurs for each sample because the derived peaks represent the maximum change in slope of the IRM curve. Table 1 lists where these peaks occur and how they relate to coercivity, which ranges from 0.15 to 0.4 tesla, and generally increases with time of oxidation.

The MAX UnMix program and the same IRM derivatives were used to calculate the relative proportions of the ferromagnetic components that contribute to the magnetic properties of the sample (Table 1). In general, magnetite dominates the magnetic signature contributing as much as 87 % of the magnetic remanence compared to 13 % contribution from hematite after only 12 minutes. Magnetite's contribution increases after 1 hour to 99 % and is consistent until the 125 hours where sample China 21 shows 95 % magnetite. This small decrease in magnetite continues in the 625-hour samples which have 94 % magnetite compared to 6 percent hematite. This small decrease in magnetite contribution after 125 hours is most likely due to magnetite converting to maghemite or hematite with increasing temperature and time (e.g., De Faria et al.

1997).

600 °C Experimental Results. Samples before and after oxidation at 600 °C were analyzed using a hysteresis loop. Each sample showed paramagnetic behavior before oxidation. Interestingly, unlike the 900 °C experiments, only the samples run for the longest times (samples SC-3 and China 1) had a ferromagnetic signature. The samples spent 625 hours oxidizing at 600 °C, and the hysteresis data is very noisy and at the detection limits of the VSM. The magnetic signature of the samples is similar to the results of Olivine-22 and SC-6 which spent only 12 minutes (0.2 hours) at 900 °C. The H_{sat} values are difficult to determine for these samples because the data is so noisy, but 0.1 to 0.2 tesla is a reasonable estimate. Following the same steps as the 900 °C, coercivity in this sample was tested using the IRM data. The normalized IRM data for the samples demonstrates the presence a ferromagnetic phase similar to the 0.2 hour 900 °C samples. Taking the first derivative for Sc-3 and China 11 shows coercivity peaks at 0.24 and 0.35 tesla, respectively. These values correspond to a presence of magnetite. Because of the high noise levels for the data for our 600 °C experiments, UnMix was not used to calculate the mineralogy.

Domain of the Magnetite Grains. The magnetic ratios of Mr/Ms versus Hcr/Hc were plotted in a logarithmic scale to inform the domain state of the magnetic grains (Dunlop 2002). In this experiment, magnetite grains formed along dislocations dominate the magnetic signature while hematite, although present chemically, has a negligible contribution. Figure 6 shows a Dunlop (2002)-style graph for our results, and indicates that most magnetite grains are single domain (SD) to pseudo-single domain (PSD). The samples that spent a longer time at 900 °C trend towards a more single domain-like behavior and a smaller grain size. This corresponds to a proportionally larger Ms value than Mr with respect to time. The 600 °C samples that produced

ferromagnetic signatures are separated from the 900 °C with a higher Hcr/Hc value correlating to an increased grain size.

Discussion

Our results show rapid olivine oxidation and alteration at both 600 and 900 °C, forming magnetite and hematite. The oxides nucleate along dislocations and impurities in the crystal structure, along with surface coatings and within cracks in the crystals. Interestingly, our results are consistent with both hematite and magnetite formation, with Raman results showing hematite dominated assemblages (**Figure 3**) and the CSM results suggesting magnetite-dominated (**Table 1**) assemblages. The difference between the results is caused by the sensitivity of the instruments, and is consistent with magnetite dominating the magnetic signature but hematite being the main oxidation product. The upper limit of the applied field that the VSM can produce is lower than the Hsat value for hematite, which is 2.0 tesla. Therefore, the VSM will not detect hematite with a hysteresis or IRM and the results will be dominated by magnetite.

Importantly, the coercivity of magnetite in any sample can be affected by the anisotropy of the grain shape and orientation with respect to the applied fields of the VSM. As a result, our altered samples have higher coercivities with increasing time of the experiment, because the oxides formed along crystallographically oriented olivine dislocations (**Figure 2**), producing anisotropic magnetite grains. The longer the experiment ran, the more the dislocations crisscross, causing an increase in magnetite grain populations with opposite orientations. Samples with greater magnetic anisotropy need a higher applied field from the VSM to saturate magnetite's magnetic field. Therefore, samples that spent longer times in the oven developed more alteration and a higher magnetic anisotropy, consistent with these samples having larger coercivities.

Olivine oxidation has been proposed as a method for forming magnetite at the crust-mantle boundary and deeper mantle depths based on mantle xenoliths at tectonic localities with suppressed geothermal gradients (Ferré et al. 2013; Ferré et al. 2014), which would require long heating periods and slow exhumation. Our results now show that olivine oxidation and alteration occurs rapidly at both 600 and 900 °C with the rate of oxidation depending on the temperature. At higher temperatures, oxidation occurs within minutes; while at the lower temperature, oxidation occurs within weeks. Whether oxidation and formation of magnetite and hematite is happening over days or weeks, this is incredibly fast on geologic time scales for in situ mantle material, but it does make a difference in considering oxidation during ascent. Decompression of xenoliths through the mantle has been estimated at up to 90 km/hour based on water concentrations in the rims of mantle olivine, which corresponds to decompression occurring over hours and not days or weeks (Demouchy et al. 2006; Peslier et al. 2015). Therefore, if the xenolithic material is transported to the surface at temperatures ≤600 °C, the time scales are likely not long enough for oxidation and magnetite formation to occur; however, if the material is transported in an oxidized basaltic magma with temperatures ≥900 °C, then oxidation and magnetite formation could occur.

One important caveat is that our experiments were conducted at oxidation states (~ QFM +10) above those typically found in the mantle (~QFM, e.g., McCammon 2005). We chose this oxygen fugacity to promote oxidation and the formation of oxidized phases in order to investigate if it can cause a magnetic signature. We are aware that this makes direct applications to mantle processes difficult and note that instead, our results are directly applicable to oxidation after eruption and in contact with air. Further, our experimental results are comparable to oxidation from contamination with either a magmatic host or metasomatic fluids in an arc

setting: typical subduction zone magma liquidus temperatures and mantle melting temperatures are > 1000 °C (as summarized by Stern 2002; Gaetani and Grove 2003) with initial eruption temperatures (based on mineral crystallization) of ~ 900 °C (e.g., Rutherford and Hill 1993; Mullen and McCallum 2013 for Mt St Helens and Mt Baker); therefore our higher temperature experiments are applicable as an upper limit in terms of formation rates during ascent and eruption and the lower temperature results are applicable as the magmatic system cools. Further, subduction zone magmas are typically more oxidized than mantle oxidation states (Parkinson and Arculus 1999; Gaetani and Grove 2003; McCammon 2005; Kelley and Cottrell 2009). Subduction zone magmas can have an oxygen fugacity up to ~ QFM +3; this is lower than the atmospheric conditions of our experiments (~QFM +10; McCammon 2005; Gaetani and Grove 2003; Mullen and McCallum 2013). The higher oxygen fugacity of our experiments will promote oxidation and nucleation of hematite at the expense of magnetite (e.g., Swaddle and Oltmann 1980; De Boer 1999). With that caveat in mind (hematite vs magnetite), our experiments are applicable to the investigation of contamination from an oxidized arc magma during ascent and eruption on the surface.

However, in addition to the observation of magnetite occurrence alone, it is vital to investigate the geometry, textures, and location of the magnetite within the xenolith as well as its mineral assemblage. Magnetite formed by oxidation of olivine forms in three distinct locations: as coating along the periphery of grains, within cracks, and as crystallographically-oriented inclusions within a grain. Therefore, any magnetite or hematite found in mantle xenoliths in these sites is likely from oxidation on ascent. In contrast, magnetite found within an olivine grain adjacent to exsolution lamellae of other mafic phases (orthopyroxene, amphibole; see Fig. 1 of Ferré et al 2013) and at distance from grain boundaries and cracks, were likely not formed during

oxidation and presumably represent magnetite that was stable at mantle depths (Ferré et al. 2013). In terms of alteration assemblage, our samples contain both magnetite and hematite, while the natural xenolith samples are dominated by magnetite (Ferré et al. 2013). In addition, when found in the natural xenoliths, grains of magnetite only occurred within olivine and pyroxene in orientations parallel to distinct crystallographic planes (Ferré et al. 2013), in contrast to the geometries found in our experimental results, which include oxidation coatings, within cracks, as well as those along crystallographically-oriented inclusions. Finally, the IRM results are significantly different between the natural xenolith samples and our experimental results (Ferré et al. 2013; Ferré et al. 2014; Friedman et al. 2014). These differences are consistent with the magnetite found within unaltered xenoliths deriving from mantle conditions, implying that magnetite endemic to the mantle could contribute to long wave length anomalies in cratonic and other tectonic environments which have a thicker lithospheric mantle (Idoko, 2017, MS thesis).

Implications

Our results show olivine oxidation and alteration to occur within minutes to days at both 600 and 900 °C forming magnetite and hematite associated with a change from paramagnetic to ferromagnetic behavior after oxidation. The oxide phases nucleate along dislocations and impurities in the crystal structure, along with surface coatings, and within cracks in the crystals. The experimental formation of ferromagnetic behavior happens quickly compared to most geologic time scales of processes taking thousands to millions of years to complete. However, when compared with the rapid rate of xenolith decompression through the mantle, the experimental time scale (especially for our 600 °C experiments) is still *slower* than the estimated 90 km/hr decompression rate for xenoliths. Therefore, if the xenolithic material is transported to the surface at low temperatures, the time scales would not be long enough for oxidation to cause

magnetite formation or a ferromagnetic signature to occur. Alternatively, if the material is transported in a high temperature (≥900 °C) oxidized magma (>>QFM), then oxidation from reaction with the magma, atmosphere, or low to moderate temperature aqueous fluids could cause magnetite formation and a ferromagnetic signature to occur. We therefore suggest that magnetite in olivine of mantle xenoliths can represent either in situ oxidation of olivine in the mantle or during ascent, and that textural relationships and magnetic measurements can assist in distinguishing magnetite formation at depth vs. during ascent.

Acknowledgements

We would like to thank support for this project from grant NSF-EAR-1345105 to ECF, JF, and JC. We would like to thank HS student Muhammad Saad Bin Tariq for help with the electron microprobe work at the OU and undergraduate student Kevin Walsh at SIU for help the project. This work benefited from comments from two anonymous reviewers and Catherine Macris that greatly strengthened and clarified the manuscript. This is LPI contribution # XXXX.

442 **Figure Captions:**

443 **Figure 1.** Images of samples after oxidation sorted by increasing time of oxidation and (a) 900
444 °C experiments and (b) 600 °C experiments.

445 **Figure 2. (A)** Back scattered electron image of a thick section of the 900 °C experiment run for
446 625 hours showing the edge of the crystal with an iron-oxide coating, oxides forming within
447 cracks, and oxides forming within the crystal structure with perpendicular orientations. (**B**) Back
448 scattered electron image of a thick section of the 900 °C experiment run for 625 hours showing
449 oxide phases forming along cracks within the crystal, as well as within the crystal structure as
450 inclusions with perpendicular orientations. The oxides forming within the crystal formed along
451 preferred crystallographic directions within the orthorhombic olivine structure. (C) Iron X-ray
452 intensity map of the same area of the thick section as shown in (B).

453 **Figure 3.** (a) Example of Raman spectra for SC-15 and SC-14 samples oxidized at 900 °C for
454 625 hours and 600 °C for 625 hours respectively, compared with known standards. (b) Raman
455 spectra for all samples plotted vs time.

456 **Figure 4.** An example hysteresis loop for sample SC-15 before oxidation (a) and after oxidation
457 at 900 °C for 625 hours (b) showing a change from paramagnetic to ferromagentic behavior.

458 **Figure 5.** Isothermal remanent magnetization (IRM) normalized curves for representative 900 °C
459 experiments. The squareness of each curve shows the approach to magnetization of a material. A
460 sharp curve attests to a soft magnetic behavior, typically what is expected from an easy to
461 magnetize mineral such as magnetite whereas in contrast a rounded curve attests to a hard
462 magnetic behavior, such as that of a difficult to magnetize mineral, like hematite (Tauxe 1998).

463 **Figure 6.** Dunlop (2002) plot for all experimental results showing magnetic grain size
464 quantification. Hcr/Hc is the remanent coercity divided by coercive force. Mr/Ms is the

465 isothermal remanent magnetization divided by the saturation magnetization. Most samples
466 exhibit more single-domain (SD) like behavior with increased heating times and temperatures.

467 **Supplemental Figure 1.** Images of all samples before and after oxidation sorted by increasing
468 time of oxidation.

469

470

References:

Banfield JF, Veblen DR, and Jones BF (1990) Transmission electron microscopy of subsolidus oxidation and weathering of olivine. Contributions to Mineralogy and Petrology 106(1):110-123

Bowen NL (1928) The Evolution of Igneous Rocks. Princeton University Press, Princeton, N.J.

Callahan C (2009) Magnetic properties of unaltered and metasomatized mantle xenoliths from the Rio Puerco volcanic necks, NM. University of New Mexico, Albuquerque, NM

Canil D, O'Neill HSC, Pearson D, Rudnick R, McDonough W, and Carswell D (1994) Ferric iron in peridotites and mantle oxidation states. Earth and Planetary Science Letters 123(1-3):205-220

Creighton S, Stachel T, Matveev S, Höfer H, McCammon C, and Luth RW (2009) Oxidation of the Kaapvaal lithospheric mantle driven by metasomatism. Contributions to Mineralogy and Petrology 157(4):491

Dasgupta R, and Hirschmann MM (2010) The deep carbon cycle and melting in Earth's interior. Earth and Planetary Science Letters 298(1-2):1-13

Dasgupta R, Mallik A, Tsuno K, Withers AC, Hirth G, and Hirschmann MM (2013) Carbon-dioxide-rich silicate melt in the Earth's upper mantle. Nature 493:211-215 doi:doi:10.1038/nature11731

De Boer CB (1999) Rock-magnetic studies on hematite, maghemite and combustion-metamorphic rocks. Utrecht University,

De Faria D, Venâncio Silva S, and De Oliveira M (1997) Raman microspectroscopy of some iron oxides and oxyhydroxides. Journal of Raman Spectroscopy 28(11):873-878

Demouchy S, Jacobsen SD, Gaillard F, and Stern CR (2006) Rapid magma ascent recorded by water diffusion profiles in mantle olivine. Geology 34(6):429-432

Dunlop DJ (2002) Theory and application of the Day plot (Mrs/Ms versus Hcr/Hc) 1. Theoretical curves and tests using titanomagnetite data. Journal of Geophysical Research: Solid Earth 107(B3):EPM 4-1-EPM 4-22 doi:10.1029/2001jb000486

Dyar MD, McGuire AV, and Harrell MD (1992) Crystal chemistry of iron in two styles of metasomatism in the upper mantle. Geochimica et Cosmochimica Acta 56(6):2579-2586 doi:http://dx.doi.org/10.1016/0016-7037(92)90212-2

Eggleton RA, Foudoulis C, and Varkevisser D (1987) Weathering of basalt: changes in rock chemistry and mineralogy. Clays and Clay Minerals 35(3):161-169

Fegley B, Klingelhöfer G, Brackett R, Izenberg N, Kremser D, and Lodders K (1995) Basalt oxidation and the formation of hematite on the surface of Venus. Icarus 118(2):373-383

Ferré EC, Friedman SA, Martín-Hernández F, Feinberg JM, Conder JA, and Ionov DA (2013) The magnetism of mantle xenoliths and potential implications for sub-Moho magnetic sources. Geophysical Research Letters 40(1):105-110 doi:10.1029/2012gl054100

Ferré EC, Friedman SA, Martín-Hernández F, Feinberg JM, Till JL, Ionov DA, and Conder JA (2014) Eight good reasons why the uppermost mantle could be magnetic. Tectonophysics 624–625(0):3-14 doi:http://dx.doi.org/10.1016/j.tecto.2014.01.004

Friedman SA, Feinberg JM, Ferré EC, Demory F, Martín-Hernández F, Conder JA, and Rochette P (2014) Craton vs. rift uppermost mantle contributions to magnetic anomalies in the United States interior. Tectonophysics 624–625(0):15-23 doi:http://dx.doi.org/10.1016/j.tecto.2014.04.023

Gaetani GA, and Grove TL (2003) Experimental constraints on melt generation in the mantle wedge. Inside the subduction factory:107-134

Goldich SS (1938) A Study in Rock-Weathering. The Journal of Geology 46(1):17-58 doi:10.1086/624619

Goode ADT (1974) Oxidation of natural olivines. Nature 248:500 doi:10.1038/248500a0

Haggerty SE, and Sautter V (1990) Ultradeep (Greater Than 300 Kilometers), Ultramafic Upper Mantle Xenoliths. Science 248(4958):993-996 doi:10.1126/science.248.4958.993

Hanesch M (2009) Raman spectroscopy of iron oxides and (oxy) hydroxides at low laser power and possible applications in environmental magnetic studies. Geophysical Journal International 177(3):941-948

Hausrath EM, Navarre-Sitchler AK, Sak PB, Steefel CI, and Brantley SL (2008) Basalt weathering rates on Earth and the duration of liquid water on the plains of Gusev Crater, Mars. Geology 36(1):67-70 doi:DOI: 10.1130/G24238A.1

Hemant K, and Maus S (2005) Geological modeling of the new CHAMP magnetic anomaly maps using a geographical information system technique. Journal of Geophysical Research: Solid Earth 110(B12) doi:doi:10.1029/2005JB003837

Ishimaru S, Arai S, and Shukuno H (2009) Metal-saturated peridotite in the mantle wedge inferred from metal-bearing peridotite xenoliths from Avacha volcano, Kamchatka. Earth and Planetary Science Letters 284(3):352-360

Kelley KA, and Cottrell E (2009) Water and the oxidation state of subduction zone magmas. Science 325(5940):605-607

Khisina NR, Khramov DA, Kleschev AA, and Langer K (1998) Laihunitization as a mechanism of olivine oxidation. European Journal of Mineralogy:229-238

Kiseeva ES, Vasiukov DM, Wood BJ, McCammon C, Stachel T, Bykov M, Bykova E, Chumakov A, Cerantola V, Harris JW, and Dubrovinsky L (2018) Oxidized iron in garnets from

539 the mantle transition zone. Nature geoscience:DOI:10.1038/s41561-41017-40055-41567
540 doi:10.1038/s41561-017-0055-7

541 Kohlstedt DL, Goetze C, Durham WB, and Sande JV (1976) New Technique for Decorating
542 Dislocations in Olivine. Science 191(4231):1045-1046 doi:10.1126/science.191.4231.1045

543 Lafuente B, Downs RT, Yang H, and Stone N (2016) The power of databases: the RRUFF
544 project. In: Highlights in mineralogical crystallography, vol. Walter de Gruyter GmbH,

545 Luguet A, and Lorand J-P (1998) Supergene weathering and sulphur contents of basalt-hosted
546 mantle xenoliths: an appraisal from Montferrier Iherzolites (Languedoc, France). Comptes
547 Rendus de l'Academie des Sciences Series IIA Earth and Planetary Science 8(327):519-525

548 Masterton SM, Gubbins D, Müller RD, and Singh KH (2013) Forward modelling of oceanic
549 lithospheric magnetization. Geophysical Journal International 192(3):951-962
550 doi:10.1093/gji/ggs063

551 Maxbauer DP, Feinberg JM, and Fox DL (2016) MAX UnMix: A web application for unmixing
552 magnetic coercivity distributions. Computers & Geosciences 95:140-145

553 McCammon C (2005) The paradox of mantle redox. Science 308(5723):807-808

554 McGuire AV, Dyar MD, and Nielson JE (1991) Metasomatic oxidation of upper mantle
555 periodotite. Contributions to Mineralogy and Petrology 109(2):252-264

556 Mullen EK, and McCallum IS (2013) Coexisting pseudobrookite, ilmenite, and titanomagnetite
557 in hornblende andesite of the Coleman Pinnacle flow, Mount Baker, Washington: Evidence for a
558 highly oxidized arc magma. American Mineralogist 98(2-3):417-425

559 Nitsan U (1974) Stability field of olivine with respect to oxidation and reduction. J Geophys Res
560 79(5):706-711

561 Nixon PH (1987) Mantle Xenoliths. John Wiley and Sons, New York

562 Oze C, and Sharma M (2005) Have olivine, will gas: Serpentinization and the abiogenic
563 production of methane on Mars. Geophys Res Lett 32(10):L10203 doi:10.1029/2005gl022691

564 Parkinson IJ, and Arculus RJ (1999) The redox state of subduction zones: insights from arc-
565 peridotites. Chemical Geology 160(4):409-423

566 Peslier AH, Bizimis M, and Matney M (2015) Water disequilibrium in olivines from Hawaiian
567 peridotites: Recent metasomatism, H diffusion and magma ascent rates. Geochimica et
568 Cosmochimica Acta 154(Supplement C):98-117 doi:https://doi.org/10.1016/j.gca.2015.01.030

569 Rutherford MJ, and Hill PM (1993) Magma ascent rates from amphibole breakdown: an
570 experimental study applied to the 1980–1986 Mount St. Helens eruptions. Journal of
571 Geophysical Research: Solid Earth 98(B11):19667-19685

572 Stern RJ (2002) SUBDUCTION ZONES. Reviews of Geophysics 40(4):3-1-3-38
573 doi:doi:10.1029/2001RG000108

574 Swaddle TW, and Oltmann P (1980) Kinetics of the magnetite–maghemite–hematite
575 transformation, with special reference to hydrothermal systems. Canadian Journal of Chemistry
576 58(17):1763-1772 doi:10.1139/v80-279

577 Syverson DD, Tutolo BM, Borrok DM, and Seyfried WE (2017) Serpentinization of olivine at
578 300°C and 500bars: An experimental study examining the role of silica on the reaction path and
579 oxidation state of iron. Chemical Geology 475(Supplement C):122-134
580 doi:https://doi.org/10.1016/j.chemgeo.2017.11.006

581 Tauxe L (1998) Paleomagnetic Principles and Practice. Kluwer Acad., Dordrecht, Netherlands

582 Thébault E, Purucker M, Whaler KA, Langlais B, and Sabaka TJ (2010) The Magnetic Field of
583 the Earth's Lithosphere. Space Science Reviews 155(1):95-127 doi:10.1007/s11214-010-9667-6

584 Warner RD, and Wasilewski PJ (1995) Magnetic petrology of lower crust and upper mantle
585 xenoliths from McMurdo Sound, Antarctica. Tectonophysics 249(1):69-92

586 Wasilewski P, and Mayhew M (1992) The Moho as a magnetic boundary revisited. Geophysical
587 Research Letters 19(22):2259-2262

588 Wasilewski PJ, Thomas HH, and Mayhew MA (1979) The Moho as a magnetic boundary.
589 Geophysical Research Letters 6(7):541-544 doi:10.1029/GL006i007p00541

590

This is a preprint, the final version is subject to change, of the American Mineralogist (MSA)
Cite as Authors (Year) Title. American Mineralogist, in press.
DOI: https://doi.org/10.2138/am-2019-6829

Table 1. Experimental oxidation conditions (time and temperature), mineralogy, an

Sample #	Experimental Conditions		Raman Spe
	T ° C	*Time (hours)*	*Mineralogy*
SC-9	900	625	Forsterite, Hematite
SC-15	900	625	Forsterite, Hematite
China 20	900	125	Forsterite, Hematite, Magnetite
China 21	900	125	N.A.
China 12	900	25	N.A.
China 17	900	25	Forsterite, Hematite, Clinohumite
SC-5	900	5	Forsterite
SC-23	900	5	N.A.
China 1	900	1	Forsterite
SC-7	900	1	Forsterite
SC-2	900	0.2	Forsterite
SC-6	900	0.2	Forsterite
SC-14	600	625	Forsterite
SC-3	600	625	Forsterite
China 2	600	125	Forsterite
China 11	600	125	Forsterite
SC-8	600	25	N.A.
SC-4	600	25	Forsterite
China 18	600	5	Forsterite
China 25	600	5	Forsterite
China 19	600	1	Forsterite
SC-24	600	1	Forsterite
SC-13	600	0.2	Forsterite
SC-16	600	0.2	Forsterite

N.D. = Not detected
N.A. = Not analyzed
Mineralogy = detection through crystal sluth > 70% match
Minor minerals = detection through crystal sluth < 70% match
All Raman peaks were matched by hand after running the peak searching function. Ar
*IRM unmix results shows the percent of magnetic contribution from each ferromagr

This is a preprint, the final version is subject to change, of the American Mineralogist (MSA)
Cite as Authors (Year) Title. American Mineralogist, in press.
DOI: https://doi.org/10.2138/am-2019-6829

d VSM results

ectrscopy	**VSM results**		**IRM Unmi**
Minor Minerals	*Hs (T) - hysteresis*	*Magnetic Phase*	*% Magnetite*
Clinohumite, Enstatite, Quartz	0.4	Magnetite	94
Clinohumite, Enstatite	0.325	Magnetite	94
Clinohumite	0.22	Magnetite	95
	0.2	Magnetite	99
	0.3	Magnetite	99
	0.245	Magnetite	99
Hematite	0.26	Magnetite	99
	0.225	Magnetite	95
Hematite	0.19	Magnetite	96
Hematite	0.225	Magnetite	90
Hematite	0.12	Magnetite	87
Hematite	0.36	Magnetite	71
Hematite, Magnetite	N.D.	N.D.	N.D.
Hematite, Clinohumite	0.125	Magnetite	N.D.
	N.D.	N.D.	N.D.
	N.D.	N.D.	N.D.
	N.D.	N.D.	N.D.
	N.D.	N.D.	N.D.
	N.D.	N.D.	N.D.
	N.D.	N.D.	N.D.
	N.D.	N.D.	N.D.
	N.D.	N.D.	N.D.
	N.D.	N.D.	N.D.
	N.D.	N.D.	N.D.

ıy phase not relevant was ignored.
ıetic phase.

This is a preprint, the final version is subject to change, of the American Mineralogist (MSA)
Cite as Authors (Year) Title. American Mineralogist, in press.
DOI: https://doi.org/10.2138/am-2019-6829

x Results*
% Hematite
6
6
5
1
1
1
1
5
4
10
13
29
N.D.
N.D.
N.D.
N.D.
N.D.
N.D.
N.D.
N.D.
N.D.
N.D.
N.D.
N.D.

This is a preprint, the final version is subject to change, of the American Mineralogist (MSA)
Cite as Authors (Year) Title. American Mineralogist, in press.
DOI: https://doi.org/10.2138/am-2019-6829

Figure 1.

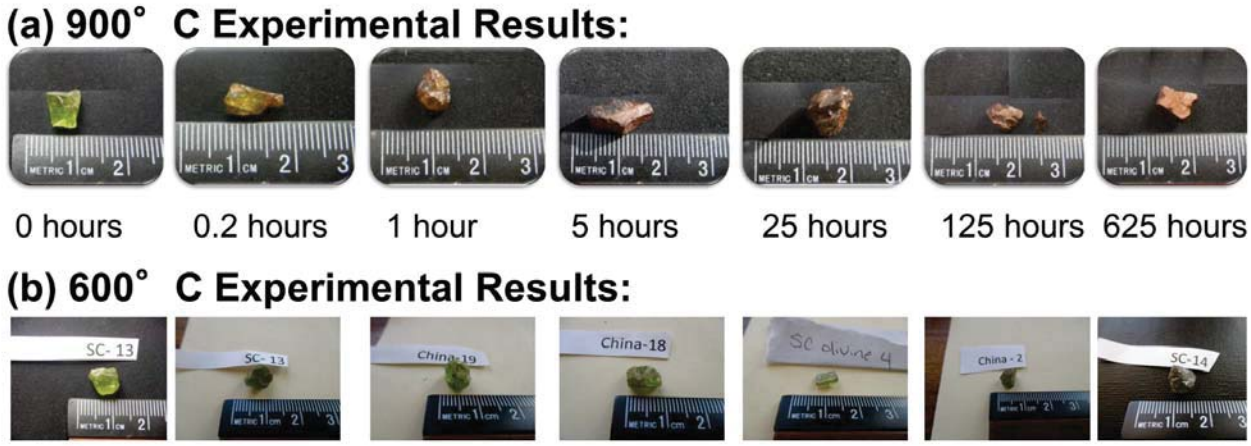

This is a preprint, the final version is subject to change, of the American Mineralogist (MSA)
Cite as Authors (Year) Title. American Mineralogist, in press.
DOI: https://doi.org/10.2138/am-2019-6829

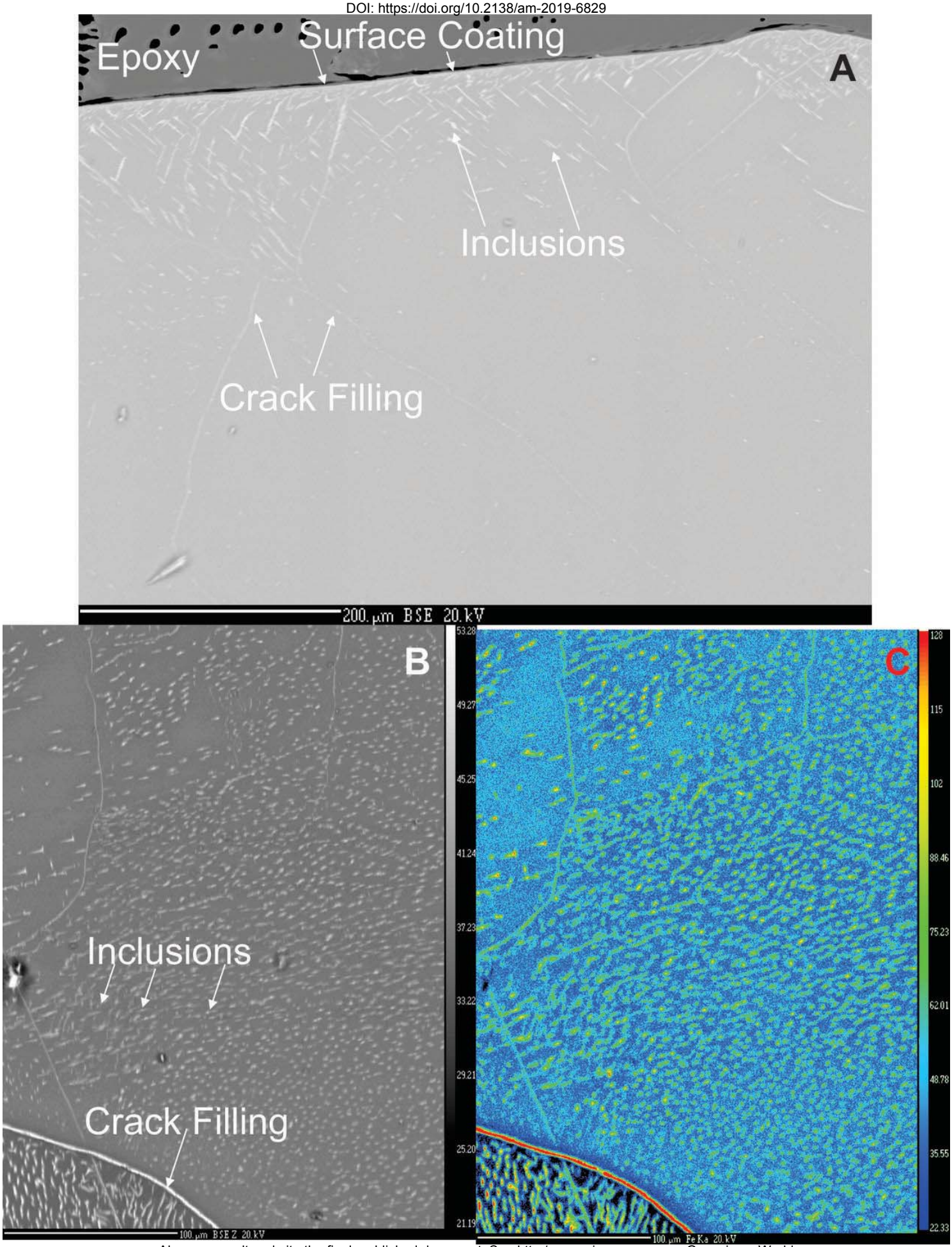

This is a preprint, the final version is subject to change, of the American Mineralogist (MSA)
Cite as Authors (Year) Title. American Mineralogist, in press.
DOI: https://doi.org/10.2138/am-2019-6829

Figure 3a.

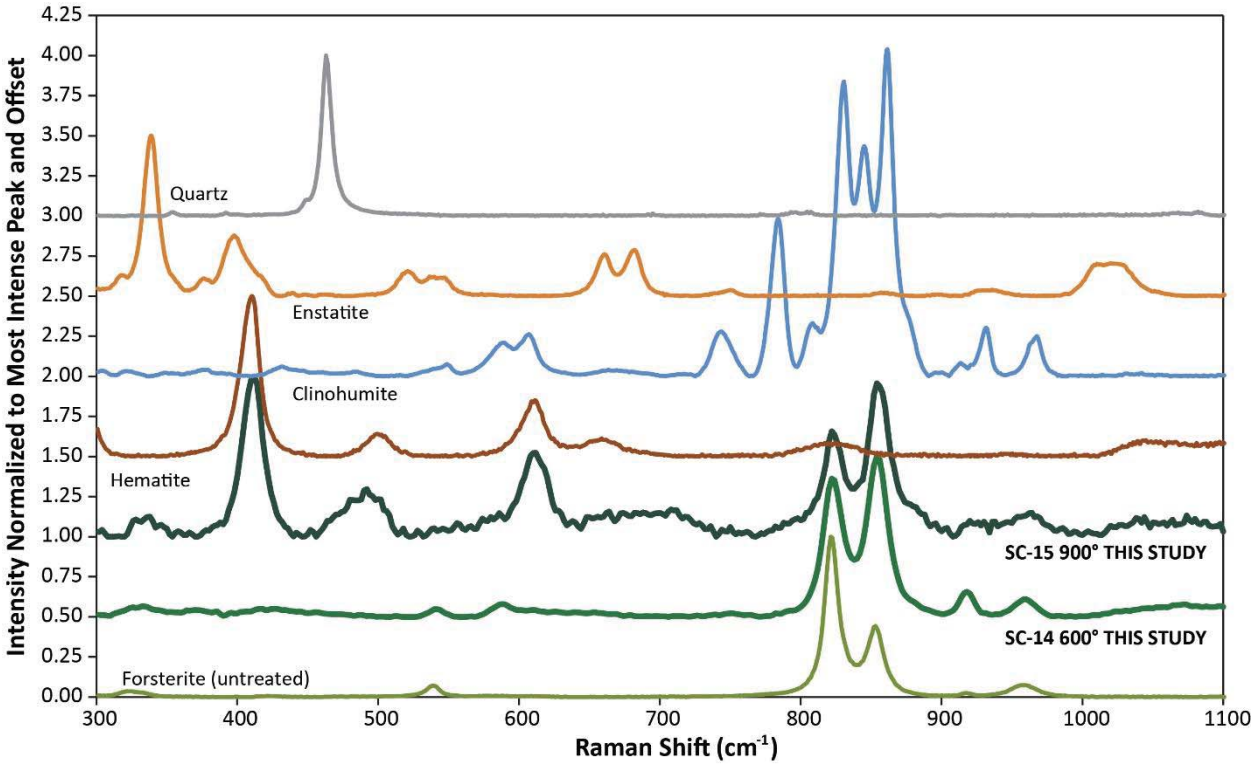

This is a preprint, the final version is subject to change, of the American Mineralogist (MSA)
Cite as Authors (Year) Title. American Mineralogist, in press.
DOI: https://doi.org/10.2138/am-2019-6829

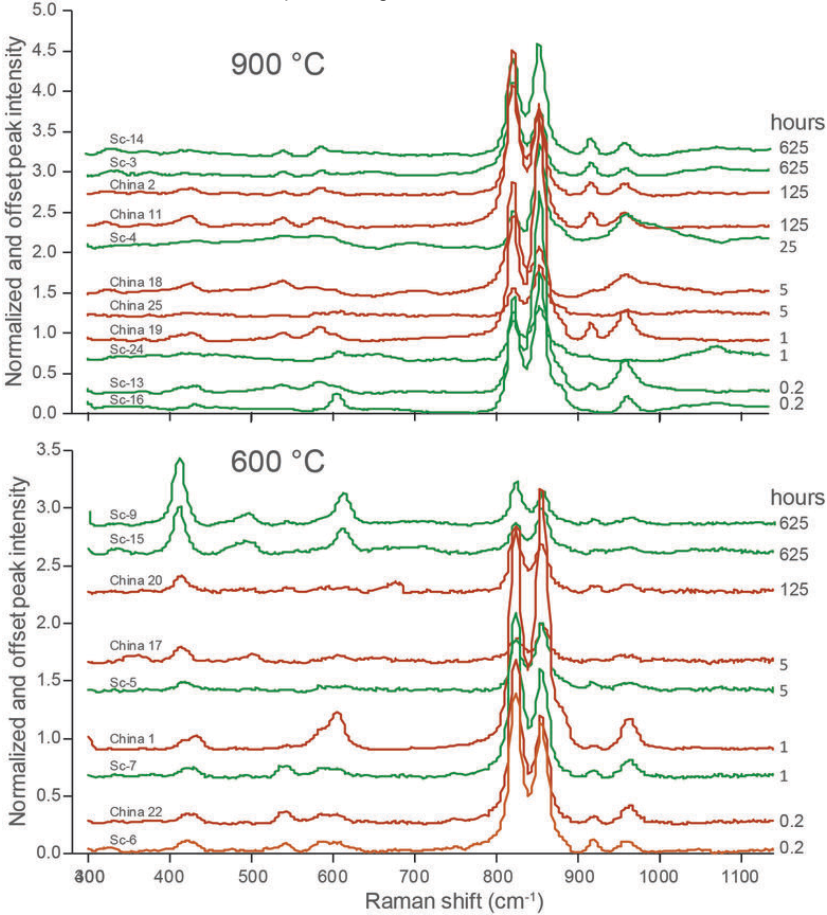

This is a preprint, the final version is subject to change, of the American Mineralogist (MSA)
Cite as Authors (Year) Title. American Mineralogist, in press.
DOI: https://doi.org/10.2138/am-2019-6829

Figure 4

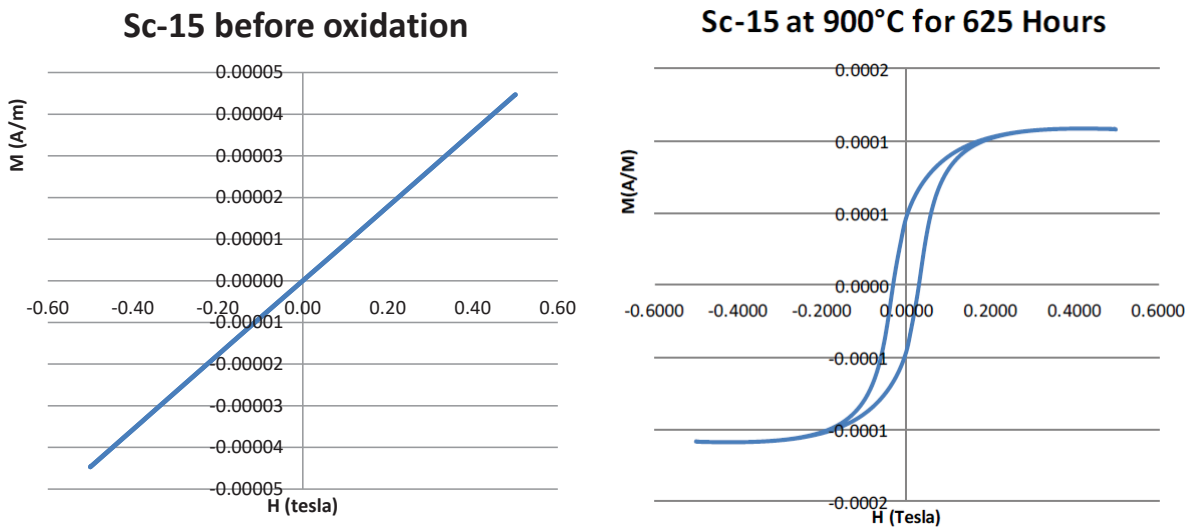

This is a preprint, the final version is subject to change, of the American Mineralogist (MSA)
Cite as Authors (Year) Title. American Mineralogist, in press.
DOI: https://doi.org/10.2138/am-2019-6829

Figure 5.

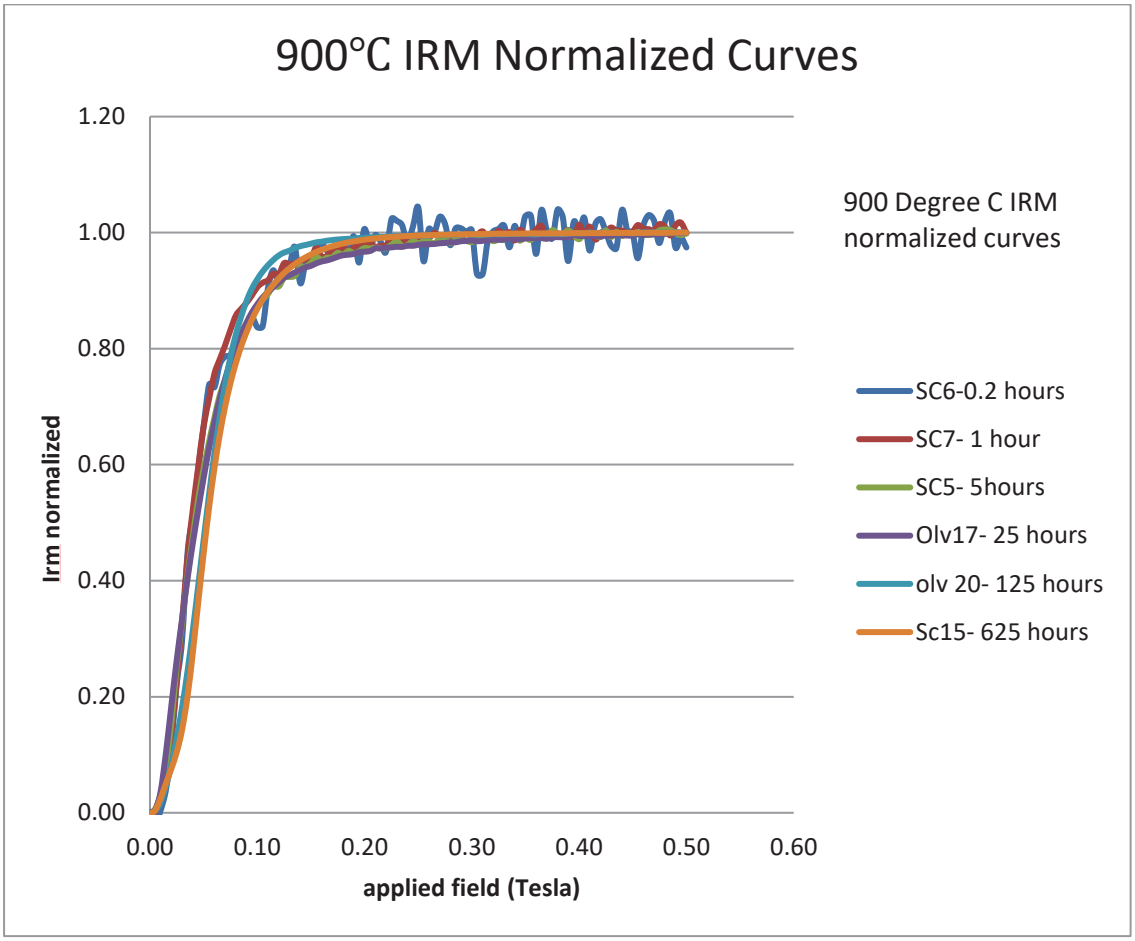

This is a preprint, the final version is subject to change, of the American Mineralogist (MSA)
Cite as Authors (Year) Title. American Mineralogist, in press.
DOI: https://doi.org/10.2138/am-2019-6829

Figure 6

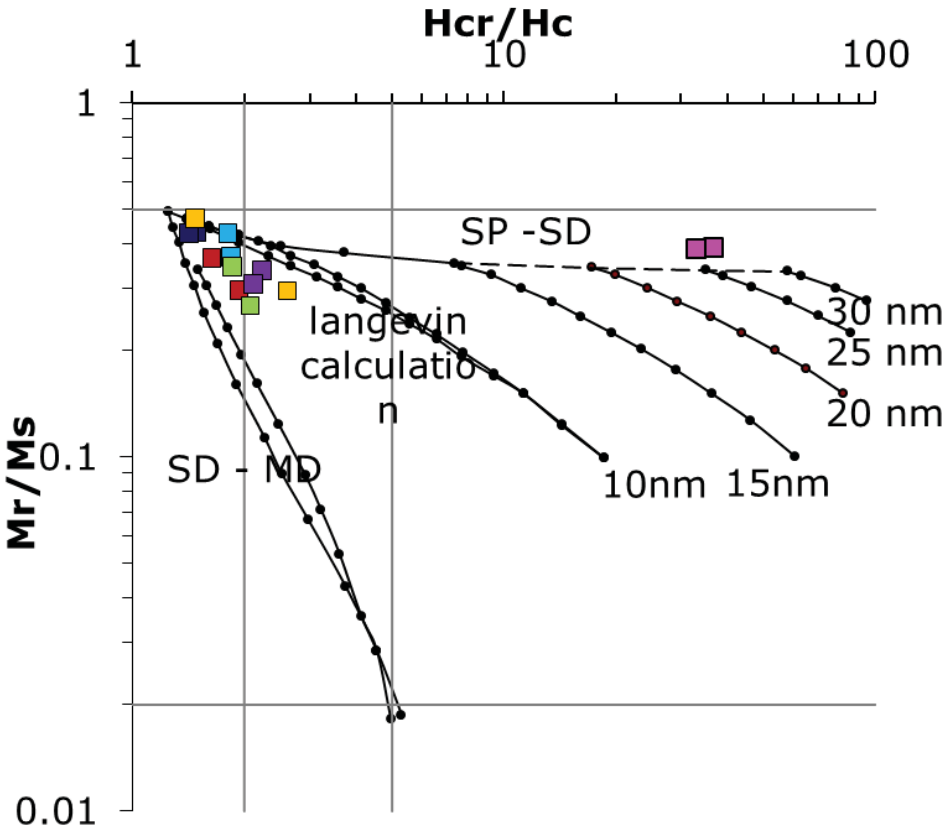

Sample #	time (hours)	Temperature (C°)
Sc-9	625	900
Sc-15	625	900
China 20	125	900
China 21	125	900
China 12	25	900
China 17	25	900
Sc-5	5	900
Sc-23	5	900
China 1	1	900
Sc-7	1	900
China 22	0.2	900
SC-6	0.2	900
Sc-14	625	600
Sc-3	625	600